Structural Instability Driven by Li/Na Competition in Na(Li_1/3Ir_2/3)O_2 Cathode Material for Li-Ion and Na-Ion Batteries

Arnaud Perez, Gwenaëlle Rousse, Jean-Marie Tarascon

Structural instability driven by Li/Na competition in $Na(Li_{1/3}Ir_{2/3})O_2$ cathode material for Li-ion and Na-ion batteries

Arnaud J. Perez[1,2,3], Gwenaëlle Rousse[1,2,3] and Jean-Marie Tarascon[1,2,3*]

[1]Collège de France, Chimie du Solide et de l'Energie, UMR 8260, 11 place Marcelin Berthelot, 75231 Paris Cedex 05, France

[2]Sorbonne Université, 4 Place Jussieu, F-75005 Paris, France

[3]Réseau sur le Stockage Electrochimique de l'Energie (RS2E), FR CNRS 3459, France

* Corresponding author: jean-marie.tarascon@college-de-france.fr

ABSTRACT

With increasing hopes placed on the Na-ion battery technology to complement the current Li-ion battery systems, it is important to improve the energy density of Na-based cathode materials. Na-rich rocksalt oxides, $Na_{1+x}M_{1-x}O_2$ (M = transition metal), combining cationic and anionic redox activity, could provide the necessary increase in capacity to achieve this goal, but their synthesis remains challenging compared to the Li analogues. As an alternative, mixed compounds $Na(A_xM_{1-x})O_2$ with A being an electropositive cation such as Li, Mg or Zn sitting in the transition metal layer, have been reported. As a continuation, we herein prepared the mixed $Na(Li_{1/3}Ir_{2/3})O_2$ phase and compared its structure and electrochemical properties with the well-known Li_2IrO_3 and Na_2IrO_3 parent materials. By mixing Na and Li in the material, the stacking sequence of the transition metal honeycomb layers in $Na(Li_{1/3}Ir_{2/3})O_2$ is modified compared to the two parent material, resulting in the presence of extra superstructure peaks in X-ray diffraction data. Using electrochemical characterization and *in situ* X-ray diffraction technique, the mixed $Na(Li_{1/3}Ir_{2/3})O_2$ was found to be unstable both in Li and Na batteries and separate into Na-rich Na_xIrO_3 and Li-rich Li_xIrO_3 phases due to the competition between electrochemical (de)insertion, cation exchange with the electrolyte, and segregation of Na and Li in the material. These findings highlight important challenges and offer useful insight to guide the design of new mixed $Na(A_xM_{1-x})O_2$ cathode materials with high capacity for Na-ion batteries.

INTRODUCTION

Designing new cathode materials for Li/Na-ion batteries with improved performances is a key challenge to achieve a successful transition to renewable energies. The search for high capacity electrodes has recently led to a paradigmatic change in charge storage mechanism with the discovery of anionic redox activity in the family of Li-rich layered transition metal oxides $Li(Li_xM_{1-x})O_2$.[1] In Li-rich materials, oxygen anions are coordinated by two or less transition metal cations, leaving non-bonding oxygen 2p orbitals located on top of the M-O bonding orbitals.[2,3] Upon Li deinsertion and oxidation of the transition metals, non-bonding oxygen levels rise to the Fermi level and become available to give electrons, thus acting as reversible redox centers. Recent reports have shown that oxygen redox is not restricted to Li-rich materials and replacing transition metals, which form covalent M-O bonds, by more electropositive species, to form ionic interactions, can be considered as a general design rule to create redox active non-bonding oxygen levels and increase the capacity of cathode materials.[3] This is particularly interesting for Na-ion cathode materials that suffer a lower energy density compared to Li-ion electrode materials. Early examples comprise the generalization of anionic redox to Na-rich materials such as Na_2RuO_3 and Na_2IrO_3.[4–6] Substituting large Na-ions in the transition metal sites is however difficult with 3d metals due to the large size mismatch. An alternative to alleviate this difficulty has been rooted in preparing mixed Na/Li compounds such as in P2-$Na_{0.6}(Li_{0.2}Mn_{0.8})O_2$.[7,8] More recent work on P2-$Na_{0.67}(Mg_{0.28}Mn_{0.72})O_2$[9,10] and P2-$Na_{2/3}(Mn_{1-y}Zn_y)O_2$[11] have also shown that alkaline-earth and d^{10} transition metal substitutions form similar ionic interaction to Li/Na, resulting in oxygen activity. Another interesting example is the cation-deficient $Na_{4/7}(\square_{1/7}Mn_{6/7})O_2$ phase,[12] in which cation vacancies also result in non-bonding oxygen states and reversible oxygen redox activity. These examples illustrate a wide range of opportunities for solid-state chemists to prepare new anionic

redox active phases. Similarly, they also raise several questions about how this new element will affect i) cation ordering, ii) the mobility of other ions during cycling, as well as iii) the stability of the oxidized material.

In this work, we investigate how the mixed Na/Li phase $Na(Li_{1/3}Ir_{2/3})O_2$, also written $Na_{1.5}Li_{0.5}IrO_3$, behaves during cycling in Li and Na cells, by comparing its electrochemical properties to the well characterized model materials Na_2IrO_3 and Li_2IrO_3.[6,13] By using iridium, we can minimize issues such as oxygen release and transition metal migrations and therefore solely focus on the interplay between Na and Li in the material.

EXPERIMENTAL

Synthesis: $Na_{1.5}Li_{0.5}IrO_3$ was synthesized using metallic Ir (Alfa Aesar, 325 mesh, 99.9%), Li_2CO_3 and Na_2CO_3 (Sigma Aldrich, 99.5%) in stoichiometric quantities. The precursors were thoroughly hand ground using a mortar and pestle and heated in air at 800°C for 48h, followed by a second heating at 900°C for 24 h, in a covered alumina crucible. After each step, the furnace was cooled to 600°C and the sample was quickly transferred to an argon-filled glovebox to avoid reaction with moisture or carbon dioxide from the air upon cooling. As for the parent compound Na_2IrO_3,[14] $Na_{1.5}Li_{0.5}IrO_3$ decomposes under ambient atmosphere, therefore all subsequent manipulations were done under argon.

Electrochemical characterization: Electrochemical characterization was performed in Swagelok-type cells. The positive electrode consisted of a laminated mixture of active material ($Na_{1.5}Li_{0.5}IrO_3$), conductive carbon (Csp) and binder (polytetrafluoroethylene, PTFE) in proportions 85:10:5 by weight. For *ex situ* characterization, the active material was simply mixed with 10 wt% Csp and used as a powder. Active material loadings were typically between 5 and 10 mg. For the Li-ion battery tests, metallic Li was used as the anode and LP30 as the electrolyte (1M $LiPF_6$ in ethylenecarbonate (EC) : dimethylcarbonate (DMC) with 1:1 ratio). For the Na-ion battery tests, metallic Na was used and 1M $NaPF_6$ in EC:DMC (1:1) with 1 wt% fluoroethylenecarbonate (FEC) additive for the electrolyte. The positive and negative electrodes were separated by two Whatman GF/D borosilicate glass fiber membranes soaked with the electrolyte for a total volume of electrolyte that can be estimated to 250-500 µL. All parts were assembled in an Ar-filled glovebox. Galvanostatic cycling was performed at a C/10 rate (1 Li^+/Na^+ exchanged in 10h, considering the chemical formula $Na_{1.5}Li_{0.5}IrO_3$) between 1.3 and 4.5 V versus

Li^+/Li, and between 2 and 4.2 V versus Na^+/Na. After cycling, samples for *ex situ* characterization were recovered inside the glovebox and washed three times in anhydrous DMC.

X-ray and Neutron Powder Diffraction experiments: Synchrotron X-ray diffraction (SXRD) was performed on *ex situ* samples at the 11-BM beamline (Advanced Photon Source, Argonne National Laboratory) with a wavelength of 0.414 Å, using sealed glass capillaries to prevent air exposure. Neutron Diffraction (ND) patterns were measured for the pristine material on the D1B powder diffractometer (Institut Laue-Langevin) with a wavelength λ = 1.2882 Å. Samples were loaded in sealed Ø=5mm vanadium cylindrical cans in an argon-filled glovebox. The strong absorption of neutron and X-ray by Ir was considered to prepare the samples and during the refinements. *In situ* XRD was performed using an electrochemical cell equipped with a Be window on a BRUKER D8 Advance diffractometer with Cu Kα radiation ($\lambda_{K\alpha1}$=1.54056 Å, $\lambda_{K\alpha2}$=1.54439 Å). Rietveld refinements were done using the FullProf suite[15].

RESULTS AND DISCUSSION

Structure of $Na_{1.5}Li_{0.5}IrO_3$.

Layered honeycomb iridates have been raising large interest in the condensed matter physic field as they display interesting magnetic properties. In 2013, Cao *et al.* reported the synthesis of single crystals of $(Na_{1-x}Li_x)_2IrO_3$ $(0 < x < 0.9)$ with different Na/Li ratio, suggesting a solid-solution between Na_2IrO_3 and Li_2IrO_3.[16] In a later report however, Manni *et al.* disproved the existence of the solid-solution by failing in their attempt to reproduce the results and by showing, through DFT calculations, that only the $x = 0.25$ composition ($Na_{1.5}Li_{0.5}IrO_3$) is stable.[17] Our own results are consistent with the work of Manni *et al*., as we succeeded in preparing only the $Na_{1.5}Li_{0.5}IrO_3$ phase while all the other compositions we tried gave mixtures of Na_2IrO_3, Li_2IrO_3 and IrO_2. This phase is very sensitive to moisture and CO_2 and needs to be handled under Ar to avoid its decomposition in air once synthesized, alike the parent Na_2IrO_3 phase. Under such precautions, a pure phase was obtained with very good crystallinity. The first Rietveld refinement using laboratory XRD data were done using the same *C*2/*m* space group as for the parent compounds, with cell parameters intermediate between Na_2IrO_3 and Li_2IrO_3. However, some small peaks were not indexed by this structural model, suggesting that the *C*2/*m* space group and unit cell are not adapted to this material. To get more precise information on the structure, synchrotron X-ray diffraction and neutron diffraction were measured on this compound.

The synchrotron data clearly shows a larger number of Bragg reflections (Figure 1a) which were not seen at first on the data collected in laboratory sources. These peaks arise from a higher order superstructure compared to the ideal 3-layer stacking sequence of honeycomb layers in Li_2IrO_3 and Na_2IrO_3,[6,13] which are usually described as O3 structures using Delmas's nomenclature.[18] Similar superstructure peaks were observed and very well described in a comprehensive paper by Liu *et*

al.[19] while studying the honeycomb ordering of $Na_3Ni_2BiO_6$ with, in that case, 6 layers (6L), 9 layers (9L) and 12 layers (12L) stacking periods. According to Liu *et al.* this high-order stacking sequence is a consequence of long-range strain present in the material. During synthesis, layered materials with honeycomb ordering gradually transform from a random stacking sequence to the ideal 3L stacking sequence of the perfect O3 phase. High order stacking sequences (4L, 6L, 9L, 12L…) correspond to intermediate energy minima, and their existence should largely depend on the reaction kinetics. An example of 4 layer (4L) stacking sequence was found by McCalla *et al.* for Li_4FeSbO_6,[20] whose structure was refined using the FAULTS program.[21] In the case of $Na(Li_{1/3}Ir_{2/3})O_2$, the 6L peaks are clearly observed (inset in Figure 1a), whereas higher order stacking sequences (9L, 12L) can only be guessed. This situation is simply described by using the structural model of Li_2SnO_3, using a *C*2/*c* space group with a unit cell twice as large as that of the parent material with *C*2/*m* symmetry, thus permitting a description of honeycomb stacking with a 6-layer periodicity (see structure in Figure 1b). Different distributions of Na and Li in the structure were investigated during the refinement using neutron diffraction data and the best result was found for Li in the center of Ir honeycombs, whereas the Na atoms occupy all the octahedral sites in the interlayer space. This is consistent with the smaller difference in effective ionic radii between Ir^{4+} (0.625 Å) and Li^+ (0.76 Å) compared to Na^+ (1.02 Å) and confirms the ordering proposed by Manni *et al.*[17] It is interesting to point out that Vallée *et al.* were recently able to prepare a layered honeycomb-ordered phase $Li_{3-x}Na_xNi_2SbO_6$ with randomly mixed Na/Li atoms in the alkali layer,[22] suggesting that the ordering of Na/Li atoms in different sites can be prevented by quenching the material from high temperature. As stacking faults are still present in the material and result in a broadening of the superstructure peak and a decrease in their intensity, we introduced some site mixing in the metallic layer between Ir and Li, in order to artificially reduce the intensity of superstructure peaks. A more in-depth study of the pristine material would require to treat the

broadening of superstructure peaks with a program able to model stacking faults, such as FAULTS.[21] The best result of neutron and synchrotron X-ray diffraction Rietveld refinement is shown in Figure 2 and the structural parameters obtained are listed in Table 1.

Electrochemical behavior of $Na_{1.5}Li_{0.5}IrO_3$ in Li cell.

The electrochemical properties of $Na_{1.5}Li_{0.5}IrO_3$ were first measured in Li cells using metallic Li as an anode and LP30 as an electrolyte (1M $LiPF_6$ in 1:1 mix of ethylcarbonate (EC) and dimethylcarbonate (DMC)). The cell was cycled at C/10 between 1.3 and 4.5 V and the cycling curve is shown in Figure 3a. Before knowing more on the mechanism, the composition of the material during cycling will be written as $(Na/Li)_xIrO_3$ with x corresponding to either Na or Li left in the material. Up to 1.5 Li^+/Na^+ can be removed on oxidation to 4.5 V, the same maximum capacity as for the parent Na_2IrO_3 and Li_2IrO_3 phases, which both undergo a phase transition to an O1 phase at the compositions $Na_{0.5}IrO_3$ and $Li_{0.5}IrO_3$, respectively. This phase transition enlists a change in the stacking of the honeycomb layers, making it impossible to remove the remaining 0.5 Na/Li ions.[6,13] Only the β polymorph of Li_2IrO_3 can be fully oxidized to IrO_3 thanks to its tridimensional structure that prevents the stabilization of some Li^+ ions.[23] The oxidation of $Na_{1.5}Li_{0.5}IrO_3$ occurs through 4 plateaus at 3.1, 3.5, 4 and 4.2 V. On discharge, the plateaus are preserved, with a very large polarization for $1.7 < x < 2.0$ in $(Na/Li)_xIrO_3$ and, surprisingly, an extra capacity on discharge around 1.4 V, with up to 0.7 extra ions inserted in the material. To ensure that this feature is not rooted in a stoichiometry issue, a second cell was assembled and started directly on discharge down to 1.3 V (red dashed line in Figure 3a). No capacity was obtained, showing that the starting stoichiometry is correct and that the extra capacity is only available after the first cycle. The multiple plateaus in the voltage curve suggest a complex structural evolution of the material upon removal of Na^+/Li^+. To assign each voltage step with the deinsertion of either Li

or Na, the differential capacity curve dQ/dV of $Na_{1.5}Li_{0.5}IrO_3$ was compared to those of Li_2IrO_3 and Na_2IrO_3 (Figure 3b). All the processes observed correlate very well with either Na or Li extraction from Na_2IrO_3 and Li_2IrO_3, respectively. Overall, it seems that Na^+ is removed first on oxidation at 3.1 V, followed by Li^+ at 3.5 V, Na^+ again at 4 V and finally Li^+ at 4.2 V. The different processes during discharge also correspond to the reduction of Na_2IrO_3 and Li_2IrO_3, with plateaus at 4.1, 3.8 and 3.4 V. However, $Na_{1.5}Li_{0.5}IrO_3$ does not show a reduction process like Na_2IrO_3 at 2.8 V, most likely because Na^+ ions get diluted in the Li^+-based electrolyte and do not reinsert in the material. There is approximately 5-20 times more Li^+ ions in the electrolyte than Na^+ ions initially in the material, and Na^+ ions present in the electrolyte are likely to plate on the anode side, thus reducing their chances to be reinserted in the material.

To understand the structural evolution of the material, *in situ* XRD was performed during a complete charge/discharge cycle vs. Li at C/10, with one pattern measured for every change in x of 0.05 in $(Na/Li)_xIrO_3$. Multiple structural changes can be seen upon cycling (Figure 3c), corresponding to each plateau in the voltage curve. One striking point is that the pristine structure (highlighted in black) is never recovered at any time during the cycling, demonstrating an irreversible evolution of the material during the first cycle. Looking more closely we found that, except for the pristine material, none of the XRD patterns could be indexed with a single phase. Instead, all patterns can be reasonably well indexed with mixtures of Na_xIrO_3 and Li_xIrO_3 at different states of charge/discharge (x = 2, 1, 0.5), suggesting that the starting material separates into two phases, one containing mostly Li, and the other mostly Na. *Ex situ* samples of the material after each plateau were prepared and measured using synchrotron X-ray diffraction to perform Rietveld analysis. The separation into two phases is clear from the refinement of the sample charged at 3.2 V, just after the first plateau. It corresponds to a mixture of O1-$NaIrO_3$ and O3-

Li_2IrO_3 (Figure 3d) and similar results are obtained for the other samples. This explains why the voltage of each plateau can be correlated so well with the voltage curves of Na_2IrO_3 and Li_2IrO_3, as shown in Figure 3b, as it simply corresponds to the superposition of the voltage curves of the Na_xIrO_3 and Li_xIrO_3 phases formed. The extra capacity obtained on reduction after a full cycle can now be understood as the insertion of extra Li^+ in Li_2IrO_3 to form a T1 structure in which interlayer octahedral sites are split into two tetrahedral sites to accommodate additional lithium. This has also been reported for $LiNiO_2$ and Li_3IrO_4 that can both be reduced to form Li_2NiO_2 and $Li_{4.7}IrO_4$, respectively.[24,25] Extra lithium insertion was not possible in the starting $Na_{1.5}Li_{0.5}IrO_3$ structure because Na in the interlayer space is too large to sit in a tetrahedral environment.

Cation exchange

To explain the decomposition reaction of the material into Na_xIrO_3 and Li_xIrO_3, two mechanisms can be imagined: the first one enlists the segregation of Li^+ and Na^+ in the sample to form Na_xIrO_3 and Li_xIrO_3 domains. The second corresponds to the exchange of Na^+ in the material with Li^+ in the electrolyte and would result in a pure Li_xIrO_3 phase with longer reaction time. Both mechanisms rely on simple chemical reactions, which do not require exchange of electrons. They can easily be tested by repeating the previous *in situ* XRD experiment while leaving the cell at open circuit voltage (OCV). In that case, XRD patterns were measured as a function of time, together with the cell voltage. The voltage curve and evolution of XRD patterns are shown in Figure 4. For the first 48 h, no change was observed, indicating that the material is stable when simply left in the Li-based electrolyte. In the meantime, the cell voltage slightly decreased, a common feature for resting cells. After 48 h, the cell was charged during 2 h at C/20 in order to remove 0.1 Na^+/Li^+ from the material and left to OCV again. Following this event, the cell voltage started to increase up to 3.3 V, well above the 3.1 V of the first plateau in the material. After stabilization of the potential, XRD

shows a phase very close to α-Li_2IrO_3 (plotted in red in Figure 4b, with α-Li_2IrO_3 plotted in dark red for comparison), with broad and asymmetric peaks indicative of the poor crystallinity of the sample. Small impurity peaks indicate the presence of some Na_xIrO_3, but in a very small amount. This experiment shows that Na^+ in the material can be exchanged with Li^+ in the electrolyte at room temperature if the material is partially oxidized to decrease the kinetic barrier for ion diffusion in and out of the material. The increase of the material's potential reflects the stabilization energy of the material upon cation exchange and can be used as a simple method to check for cation exchange in mixed Na/Li electrodes.

$Na_{1.5}Li_{0.5}IrO_3$ in Na cell

At this stage, to check the validity of the Na^+/Li^+ exchange process, a Na cell using 1M $NaPF_6$ in EC:DMC with 1% FEC as an electrolyte and Na as an anode was cycled between 2 and 4.2 V vs. Na^+/Na at C/10. As shown in Fig. 5a, the voltage curve on oxidation partially differs from that of the Li cells. The same capacity (~1.5 Na^+/Li^+) can be obtained on oxidation, but the following reduction curve shows a lower voltage compared to the Li cell with, in addition, three plateaus instead of two located at 2.8, 2.9 and 3.3 V vs. Na^+/Na for $1 \leq x \leq 2$ in $(Na/Li)_xIrO_3$. For $x \leq 1$, two processes are still visible, while the following discharge is more complex. Going to lower voltages did not result in extra Na^+ insertion as for the Li cell. To grasp further insights into this difference, an *in situ* XRD experiment was performed during the first charge/discharge cycle vs. Na (Figure 5b). It reveals a solid-solution process for $1.6 \leq x \leq 2$ in $(Na/Li)_xIrO_3$, corresponding to the formation of a new phase (highlighted in green in Figure 5b) with a structure similar to the pristine material and an increased interlayer distance, consistent with Na removal from the interlayer space. Note that this structural transition was barely observed during the cycling vs. Li due to the concurrent Na^+/Li^+ exchange reaction. On the next plateau, intense peaks pertaining to

a Na_xIrO_3 phase and smaller peaks from a Li_xIrO_3 phase are observed. This shows that the Na^+/Li^+ exchange reaction cannot explain by itself the decomposition of $Na_{1.5}Li_{0.5}IrO_3$ upon cycling, as previously hypothesized, which is also associated to a segregation of Li and Na in the structure at 2.9 V vs Na^+/Na (or 3.2 V vs Li^+/Li in a Li cell). The peaks of the Li_xIrO_3 phase are however less intense here compared to the Li cell as the exchange reaction is prevented. This is also consistent with the smaller capacity obtained on oxidation at 3.2 V vs Li^+/Li from Li deinsertion, compared to the large plateau at 3.5 V vs Na^+/Na in the Na cell (Figure 3a), as more lithium is available after the exchange process than is initially present in the pristine material. Interestingly, the fully charged material, after removing 1.5 Na/Li, is very similar to that obtained in the Li cell, again with a lower contribution of the Li_xIrO_3 phase. On the next discharge, Na^+ is inserted back in the material, giving two phases at 1.5 V (Figure 5c): the first one corresponding to Na_2IrO_3 and the second one with cell parameters close to the pristine $Na_{1.5}Li_{0.5}IrO_3$ phase. Lastly, it is worth mentioning that the proportion of the Na_2IrO_3 phase within the electrode, which is already the main phase after one cycle, keeps increasing with cycling. In short, by way of summary, we found that cycling $Na_{1.5}Li_{0.5}IrO_3$ in both Li and Na cells leads to a transformation of the material into two phases, one being Na-rich and the other Li-rich. The proposed mechanism for competing deinsertion/insertion of Li and Na during the first cycle is summarized in Figure 6a for a Li cell and Figure 6b for a Na cell.

CONCLUSION

We prepared a mixed Na/Li iridate phase $Na_{1.5}Li_{0.5}IrO_3$ to understand how the electropositive cation in the honeycomb layer affects the electrochemical and structural evolution of the material upon cycling. Combining synchrotron X-ray and neutron diffraction data, we found that Li prefers to sit in the center of the Ir honeycomb layer while Na remains in the interlayer space. We observed

that the mixed Na/Li phase shows a more complex stacking sequence than the parent Na_2IrO_3 and Li_2IrO_3 phases, with at least a 6-layer staking periodicity. This differs from the 3-layer periodicity of the parent phases, suggesting that mixing different electropositive cations could help in controlling the stacking of layered materials, a factor that affects the electrochemical properties of Na-based layered oxides to a large extent. The high mobility of Na^+ and Li^+ ions resulted in a complex structural evolution upon cycling in both Li and Na cells, understood using *in situ* XRD: Na/Li exchange reaction and segregation directly compete with the electrochemical (de)insertion mechanism, eventually leading to the formation of Li-rich Li_xIrO_3 and Na-rich Na_xIrO_3 phases. A further rationalization of this work calls for DFT calculations as it is being planned. However, increasing the capacity of Na layered oxides by substituting Li in the transition metal layer to activate oxygen redox is an exciting strategy, provided we can prevent such Na/Li exchange reactions. One way forward, as described in recent papers, is to use electropositive cations with lower mobility and smaller size, such as Mg^{2+} or Zn^{2+},[9–11] to increase the capacity of Na-ion cathode materials while limiting their mobility and material decomposition.

ASSOCIATED CONTENT

Accession Codes

CCDC 1952737 contains the supplementary crystallographic data for this paper. These data can be obtained free of charge via www.ccdc.cam.ac.uk/data_request/cif, or by emailing data_request@ccdc.cam.ac.uk, or by contacting The Cambridge Crystallographic Data Centre, 12 Union Road, Cambridge CB2 1EZ, UK; fax: +44 1223 336033.

AUTHOR INFORMATION

Corresponding author

E-mail: jean-marie.tarascon@college-de-france.fr

ORCID

Arnaud J. Perez: 0000-0003-1659-554X

Gwenaëlle Rousse: 0000-0001-8877-0015

Jean-Marie Tarascon: 0000-0002-7059-6845

Notes

The authors declare no competing financial interest.

ACKNOWLEDGEMENT

This work is based on experiments performed at Institut Laue Langevin, Grenoble, France. The authors would like to thank Vivian Nassif for her help in neutron diffraction experiment at the D1B diffractometer at ILL. Use of the 11-BM mail service of the APS at Argonne National Laboratory

was supported by the U.S. department of Energy under contract No. DE-AC02-06CH11357 and is greatly acknowledged.

REFERENCES

(1) Sathiya, M.; Rousse, G.; Ramesha, K.; Laisa, C. P.; Vezin, H.; Sougrati, M. T.; Doublet, M.-L.; Foix, D.; Gonbeau, D.; Walker, W.; et al. Reversible Anionic Redox Chemistry in High-Capacity Layered-Oxide Electrodes. *Nat. Mater.* **2013**, *12* (9), 827–835.

(2) Saubanère, M.; McCalla, E.; Tarascon, J.-M.; Doublet, M.-L. The Intriguing Question of Anionic Redox in High-Energy Density Cathodes for Li-Ion Batteries. *Energy Environ. Sci.* **2016**, *9* (3), 984–991.

(3) Yahia, M. B.; Vergnet, J.; Saubanère, M.; Doublet, M.-L. Unified Picture of Anionic Redox in Li/Na-Ion Batteries. *Nat. Mater.* **2019**, 1.

(4) Rozier, P.; Sathiya, M.; Paulraj, A.-R.; Foix, D.; Desaunay, T.; Taberna, P.-L.; Simon, P.; Tarascon, J.-M. Anionic Redox Chemistry in Na-Rich $Na_2Ru_{1-y}Sn_yO_3$ Positive Electrode Material for Na-Ion Batteries. *Electrochem. Commun.* **2015**, *53*, 29–32.

(5) Mortemard de Boisse, B.; Liu, G.; Ma, J.; Nishimura, S.; Chung, S.-C.; Kiuchi, H.; Harada, Y.; Kikkawa, J.; Kobayashi, Y.; Okubo, M.; et al. Intermediate Honeycomb Ordering to Trigger Oxygen Redox Chemistry in Layered Battery Electrode. *Nat. Commun.* **2016**, *7*, 11397.

(6) Perez, A. J.; Batuk, D.; Saubanère, M.; Rousse, G.; Foix, D.; McCalla, E.; Berg, E. J.; Dugas, R.; H. W. van den Bos, K.; Doublet, M.-L.; et al. Strong Oxygen Participation in the Redox Governing the Structural and Electrochemical Properties of Na-Rich Layered Oxide Na_2IrO_3. *Chem. Mater.* **2016**, *28* (22), 8278–8288.

(7) Du, K.; Ryu, K.-S.; Hu, G. Layered Lithium-Sodium Manganese Oxide as a Cathode Material for Lithium Ion Batteries. *ECS Electrochem. Lett.* **2013**, *2* (4), A36–A38.

(8) de la Llave, E.; Talaie, E.; Levi, E.; Nayak, P. K.; Dixit, M.; Rao, P. T.; Hartmann, P.; Chesneau, F.; Major, D. T.; Greenstein, M.; et al. Improving Energy Density and Structural Stability of Manganese Oxide Cathodes for Na-Ion Batteries by Structural Lithium Substitution. *Chem. Mater.* **2016**, *28* (24), 9064–9076.

(9) Yabuuchi, N.; Hara, R.; Kubota, K.; Paulsen, J.; Kumakura, S.; Komaba, S. A New Electrode Material for Rechargeable Sodium Batteries: P2-Type $Na_{2/3}Mn_{0.72}]O_2$ with Anomalously High Reversible Capacity. *J. Mater. Chem. A* **2014**, *2* (40), 16851–16855.

(10) Maitra, U.; House, R. A.; Somerville, J. W.; Tapia-Ruiz, N.; Lozano, J. G.; Guerrini, N.; Hao, R.; Luo, K.; Jin, L.; Pérez-Osorio, M. A.; et al. Oxygen Redox Chemistry without Excess Alkali-Metal Ions in $Na_{2/3}[Mg_{0.28}Mn_{0.72}]O_2$. *Nat. Chem.* **2018**, *10* (3), 288–295.

(11) Bai, X.; Sathiya, M.; Mendoza-Sánchez, B.; Iadecola, A.; Vergnet, J.; Dedryvère, R.; Saubanère, M.; Abakumov, A. M.; Rozier, P.; Tarascon, J.-M. Anionic Redox Activity in a Newly Zn-Doped Sodium Layered Oxide P2-$Na_{2/3}Mn_{1-y}Zn_yO_2$ ($0 < y < 0.23$). *Adv. Energy Mater.* **2018**, *8* (32), 1802379.

(12) Boisse, B. M. de; Nishimura, S.; Watanabe, E.; Lander, L.; Tsuchimoto, A.; Kikkawa, J.; Kobayashi, E.; Asakura, D.; Okubo, M.; Yamada, A. Highly Reversible Oxygen-Redox

Chemistry at 4.1 V in $Na_{4/7-x}[\square_{1/7}Mn_{6/7}]O_2$ (□: Mn Vacancy). *Adv. Energy Mater.* **2018**, *0* (0), 1800409.

(13) McCalla, E.; Abakumov, A. M.; Saubanère, M.; Foix, D.; Berg, E. J.; Rousse, G.; Doublet, M.-L.; Gonbeau, D.; Novák, P.; Tendeloo, G. V.; et al. Visualization of O-O Peroxo-like Dimers in High-Capacity Layered Oxides for Li-Ion Batteries. *Science* **2015**, *350* (6267), 1516–1521.

(14) Krizan, J. W.; Roudebush, J. H.; Fox, G. M.; Cava, R. J. The Chemical Instability of Na_2IrO_3 in Air. *Mater. Res. Bull.* **2014**, *52*, 162–166.

(15) Rodríguez-Carvajal, J. Recent Advances in Magnetic Structure Determination by Neutron Powder Diffraction. *Phys. B Condens. Matter* **1993**, *192* (1–2), 55–69.

(16) Cao, G.; Qi, T. F.; Li, L.; Terzic, J.; Cao, V. S.; Yuan, S. J.; Tovar, M.; Murthy, G.; Kaul, R. K. Evolution of Magnetism in the Single-Crystal Honeycomb Iridates $(Na_{1-x}Li_x)_2IrO_3$. *Phys. Rev. B* **2013**, *88* (22), 220414.

(17) Manni, S.; Choi, S.; Mazin, I. I.; Coldea, R.; Altmeyer, M.; Jeschke, H. O.; Valentí, R.; Gegenwart, P. Effect of Isoelectronic Doping on the Honeycomb-Lattice Iridate A_2IrO_3. *Phys. Rev. B* **2014**, *89* (24), 245113.

(18) Delmas, C.; Fouassier, C.; Hagenmuller, P. Structural Classification and Properties of the Layered Oxides. *Phys. BC* **1980**, *99* (1–4), 81–85.

(19) Liu, J.; Yin, L.; Wu, L.; Bai, J.; Bak, S.-M.; Yu, X.; Zhu, Y.; Yang, X.-Q.; Khalifah, P. G. Quantification of Honeycomb Number-Type Stacking Faults: Application to $Na_3Ni_2BiO_6$ Cathodes for Na-Ion Batteries. *Inorg. Chem.* **2016**, *55* (17), 8478–8492.

(20) McCalla, E.; Abakumov, A.; Rousse, G.; Reynaud, M.; Sougrati, M. T.; Budic, B.; Mahmoud, A.; Dominko, R.; Van Tendeloo, G.; Hermann, R. P.; et al. Novel Complex Stacking of Fully-Ordered Transition Metal Layers in Li_4FeSbO_6 Materials. *Chem. Mater.* **2015**, *27* (5), 1699–1708.

(21) Casas-Cabanas, M.; Reynaud, M.; Rikarte, J.; Horbach, P.; Rodríguez-Carvajal, J. FAULTS: A Program for Refinement of Structures with Extended Defects. *J. Appl. Crystallogr.* **2016**, *49* (6), 2259–2269.

(22) Vallée, C.; Saubanère, M.; Sanz-Camacho, P.; Biecher, Y.; Fraisse, B.; Suard, E.; Rousse, G.; Carlier, D.; Berthelot, R. Alkali-Glass Behavior in Honeycomb-Type Layered $Li_{3-x}Na_xNi_2SbO_6$ Solid Solution. *Inorg. Chem.* **2019**.

(23) Pearce, P. E.; Perez, A. J.; Rousse, G.; Saubanère, M.; Batuk, D.; Foix, D.; McCalla, E.; Abakumov, A. M.; Van Tendeloo, G.; Doublet, M.-L.; et al. Evidence for Anionic Redox Activity in a Tridimensional-Ordered Li-Rich Positive Electrode β-Li_2IrO_3. *Nat. Mater.* **2017**, *16* (5), 580–586.

(24) Dahn, J. R.; von Sacken, U.; Michal, C. A. Structure and Electrochemistry of $Li_{1\pm y}NiO_2$ and a New Li_2NiO_2 Phase with the $Ni(OH)_2$ Structure. *Solid State Ion.* **1990**, *44* (1), 87–97.

(25) Perez, A. J.; Jacquet, Q.; Batuk, D.; Iadecola, A.; Saubanère, M.; Rousse, G.; Larcher, D.; Vezin, H.; Doublet, M.-L.; Tarascon, J.-M. Approaching the Limits of Cationic and Anionic Electrochemical Activity with the Li-Rich Layered Rocksalt Li_3IrO_4. *Nat. Energy* **2017**, *2* (12), 954.

LIST OF FIGURES

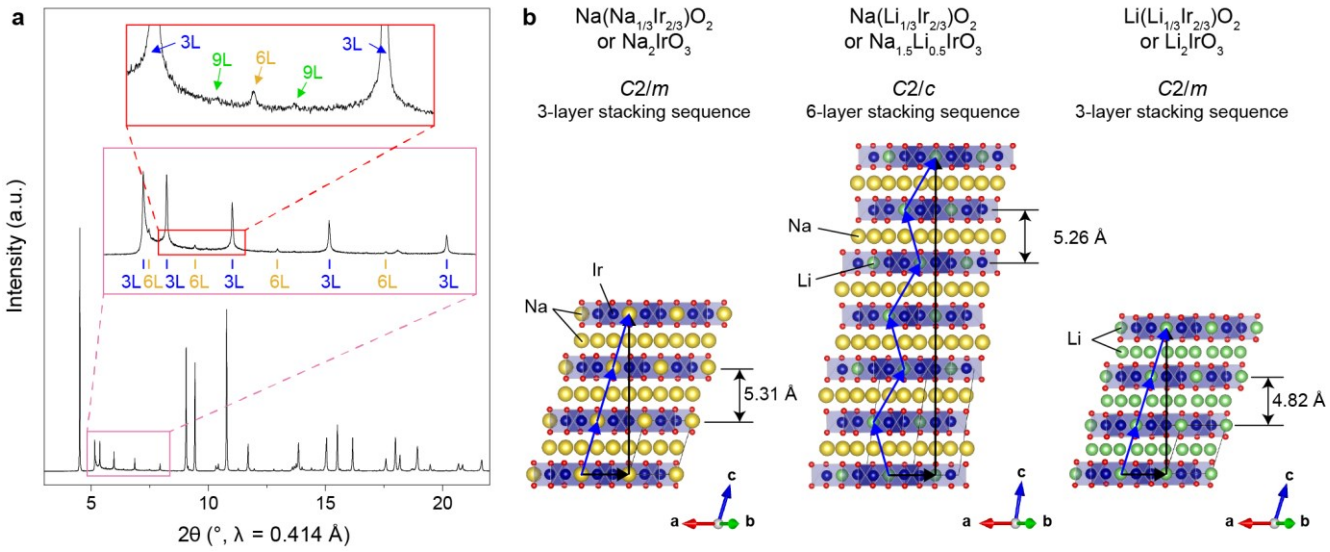

Figure 1 : (a) High order superstructure peaks observed in the synchrotron X-ray diffraction pattern of $Na_{1.5}Li_{0.5}IrO_3$. 3L, 6L and 9L indexed peaks arise from the 3-, 6- and 9-layers periodicity of the stacking sequence, respectively. (b) Structures of Na_2IrO_3, $Na_{1.5}Li_{0.5}IrO_3$ and Li_2IrO_3. The stacking periodicity of honeycomb layers is made explicit by blue and black arrows and differ between the *C*2/*m* structure of the parent materials (3-layer periodicity) and the *C*2/*c* structure of $Na_{1.5}Li_{0.5}IrO_3$ (6-layer periodicity).

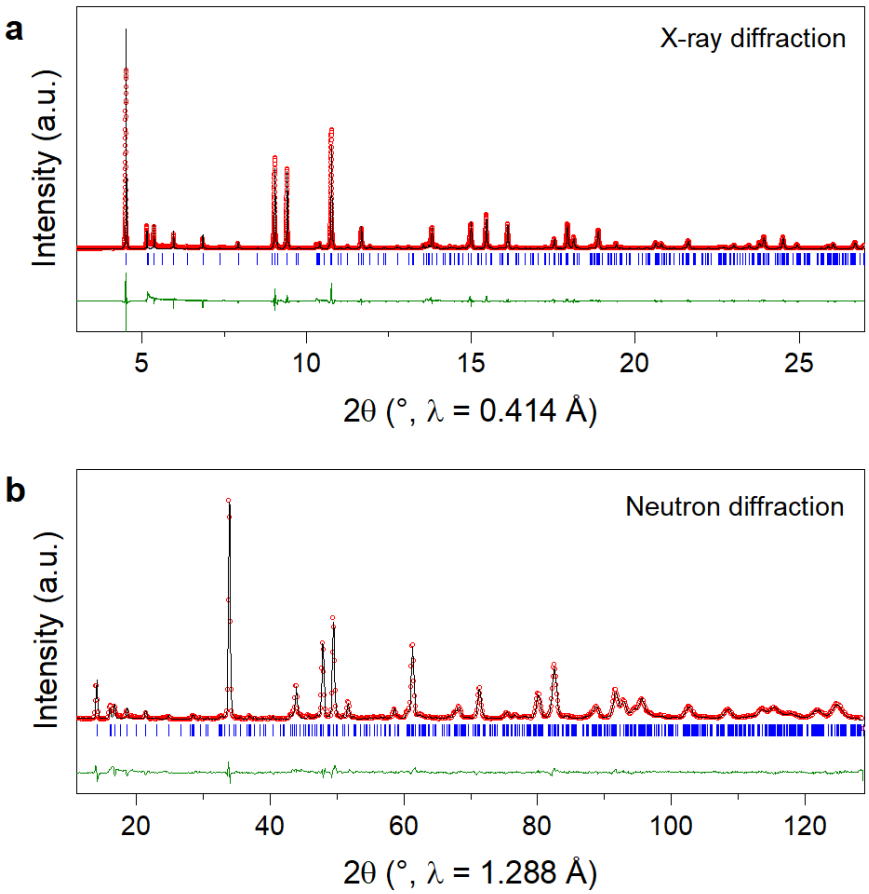

Figure 2: Rietveld refinement of diffraction data for $Na_{1.5}Li_{0.5}IrO_3$, using synchrotron X-ray (a) and neutron (b) data. Experimental points are marked by red circles, the calculated pattern by a black line, the difference between experimental and calculated patterns by a green line and the position of Bragg reflections by blue tick marks.

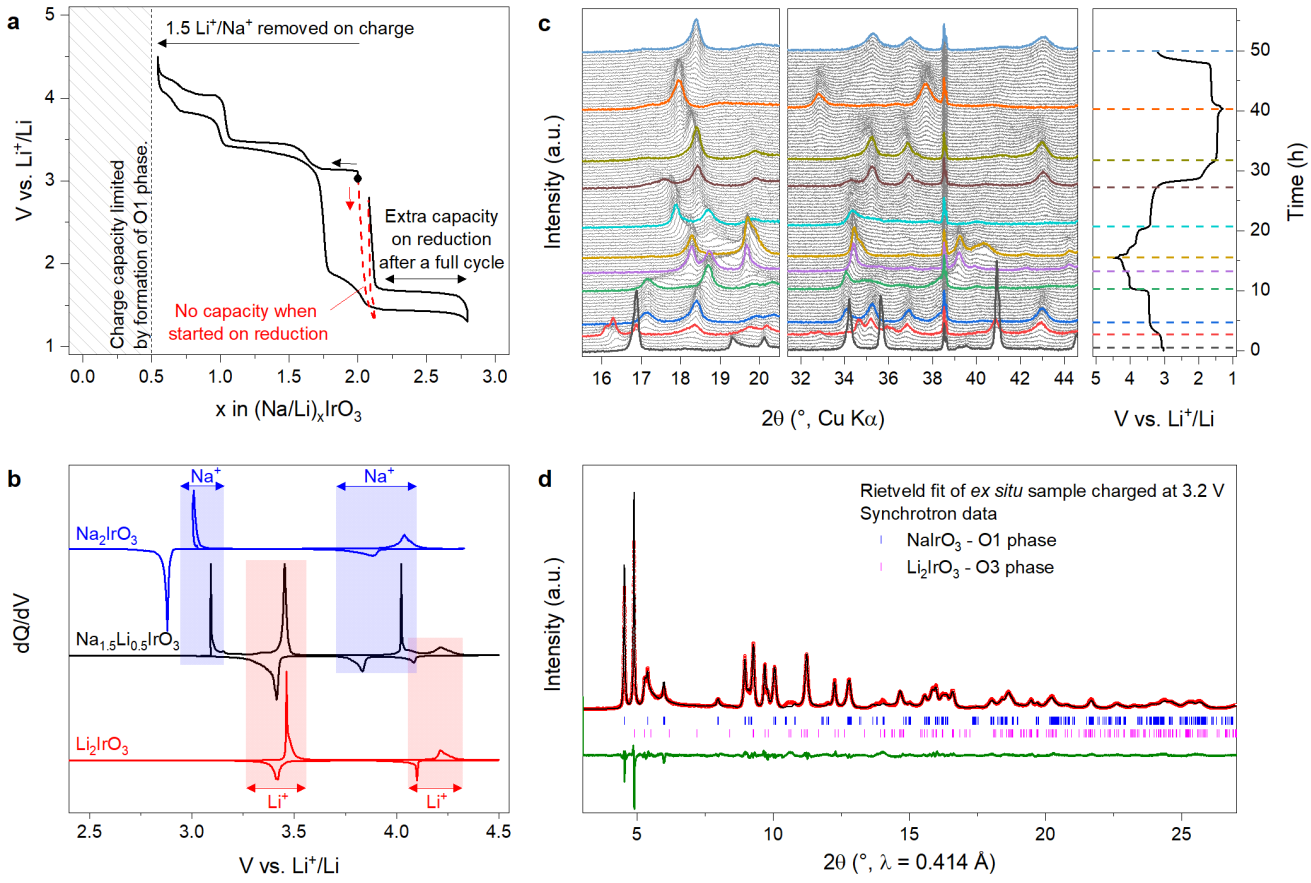

Figure 3: Cycling of $Na_{1.5}Li_{0.5}IrO_3$ in Li cell. (a) First charge/discharge cycle between 1.3 and 4.5 V vs. Li^+/Li. A second cell was started on reduction down to 1.3 V (red dashed line) but no Li^+ was inserted, in contrast with the extra insertion observed after a complete cycle. The diagonal-filled rectangle represents the inaccessible capacity if an O1 phase is formed as for Na_2IrO_3 and Li_2IrO_3. (b) Comparison between dQ/dV curves of $Na_{1.5}Li_{0.5}IrO_3$ vs. Li^+/Li and the parent materials Na_2IrO_3 and Li_2IrO_3. The dQ/dV curve of Na_2IrO_3 was measured vs Na^+/Na, and the potential was shifted by 0.33 V to match that of Li^+/Li. (c) *In situ* XRD experiment showing complex irreversible structural modifications during the first cycle. (d) Rietveld refinement of an *ex situ* sample charged at 3.2 V, corresponding to x = 1.6 in $(Na/Li)_xIrO_3$, indicates that $Na_{1.5}Li_{0.5}IrO_3$ transforms into a mixture of Na_xIrO_3 and Li_xIrO_3 as soon as the charge process starts.

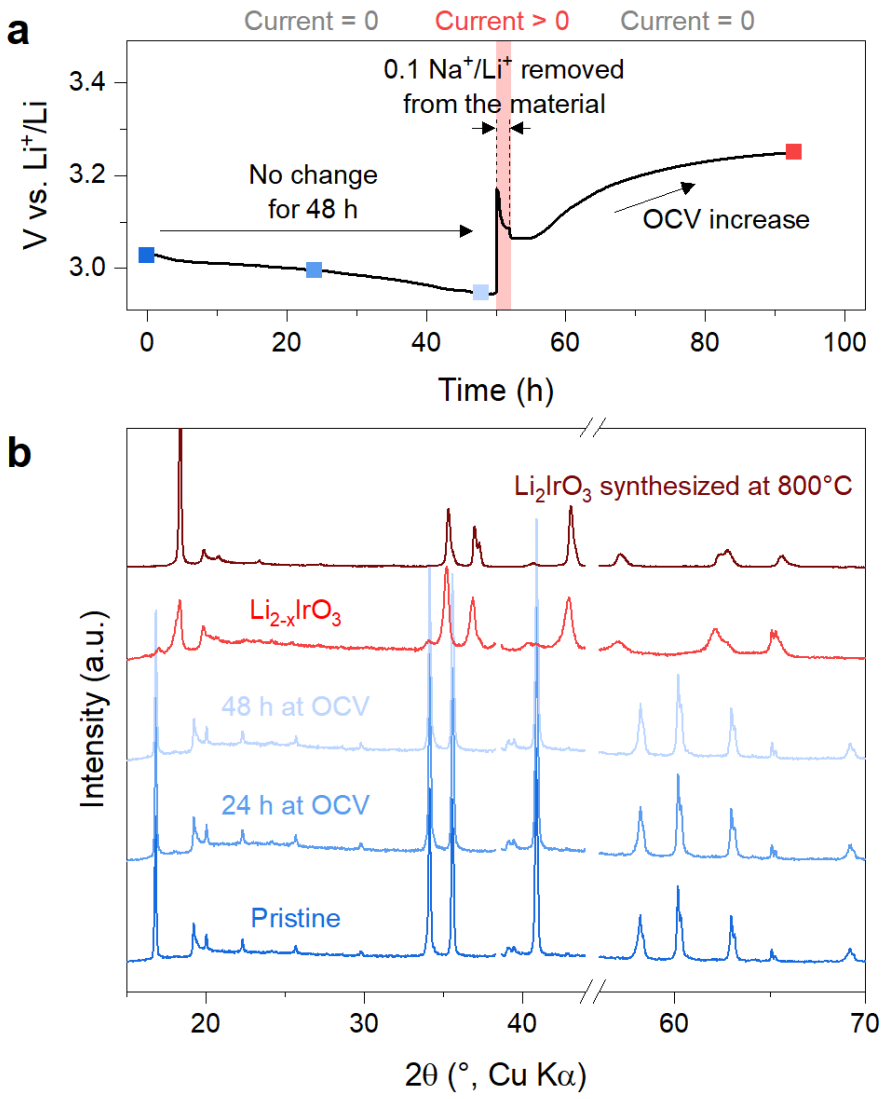

Figure 4 : XRD study of the Na^+/Li^+ exchange reaction in a Li cell. (a) The potential of the cell is measured as a function of time. The cell is first left at OCV for 48 h, then charged at C/20 for 2 h (0.1 Na^+/Li^+ removed) and finally left at OCV. (b) Selected XRD patterns obtained at different times of the experiment, indicated by square markers on the voltage curve. 2θ regions corresponding to peaks of the *in situ* cell are not plotted for clarity. A pattern of α-Li_2IrO_3 prepared by solid-state synthesis at 800°C is also plotted for comparison.

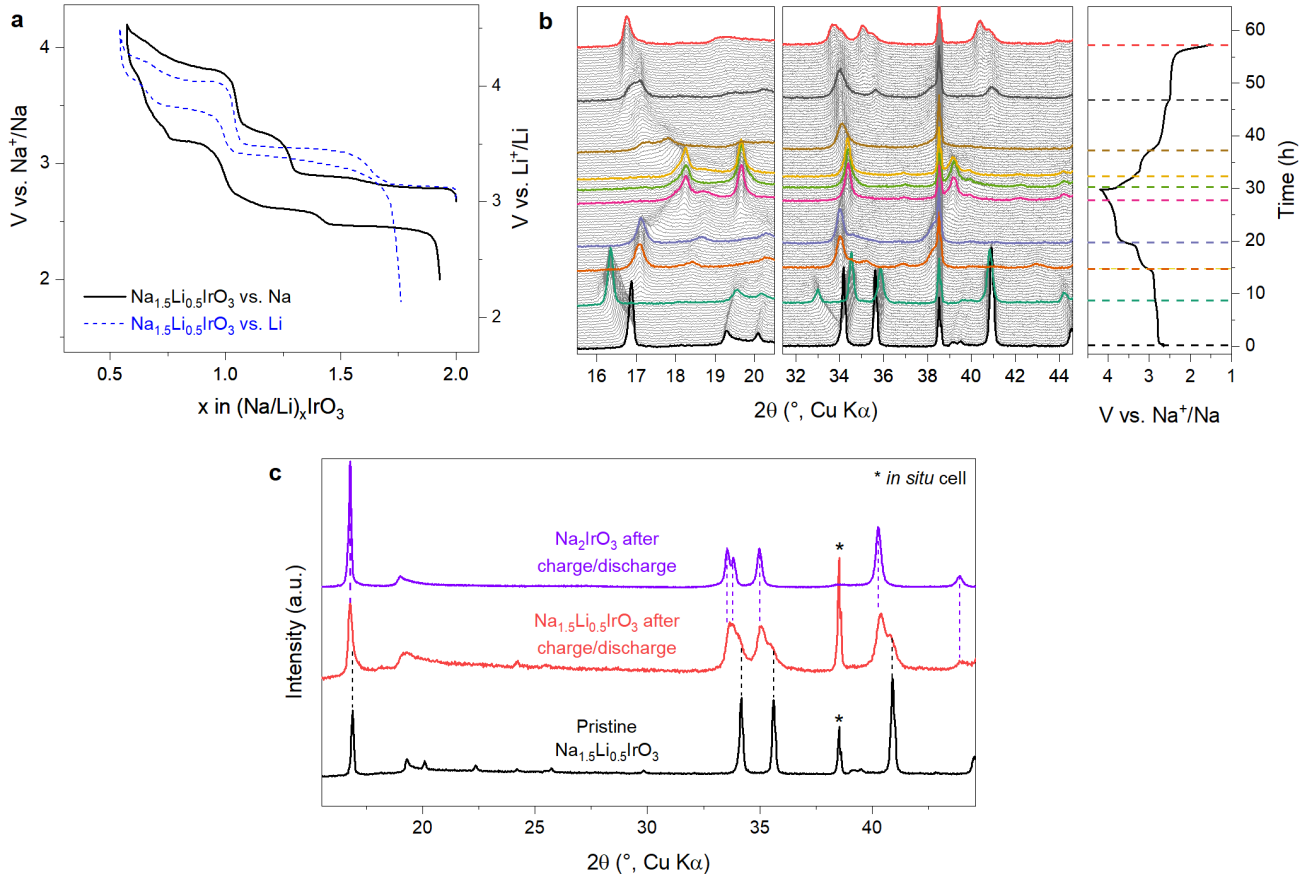

Figure 5 : Cycling of $Na_{1.5}Li_{0.5}IrO_3$ in Na cell. (a) First charge/discharge cycle between 2 and 4.2 V vs. Na^+/Na (left axis). The voltage curve in a Li cell is shown for comparison (blue dashed line, right axis) and is shifted by the potential difference between Na^+/Na and Li^+/Li. (b) *In situ* XRD study of $Na_{1.5}Li_{0.5}IrO_3$ vs. Na at a rate of C/20. Colored lines highlight the different phases obtained after each plateau. (c) XRD pattern of $Na_{1.5}Li_{0.5}IrO_3$ after a complete charge/discharge cycle vs. Na (middle), compared to the pattern of the pristine material (bottom) and that of Na_2IrO_3 cycled in the same conditions (top). The dashed lines highlight that the cycled $Na_{1.5}Li_{0.5}IrO_3$ is a mixture of the two phases, suggesting a segregation of Na and Li during cycling.

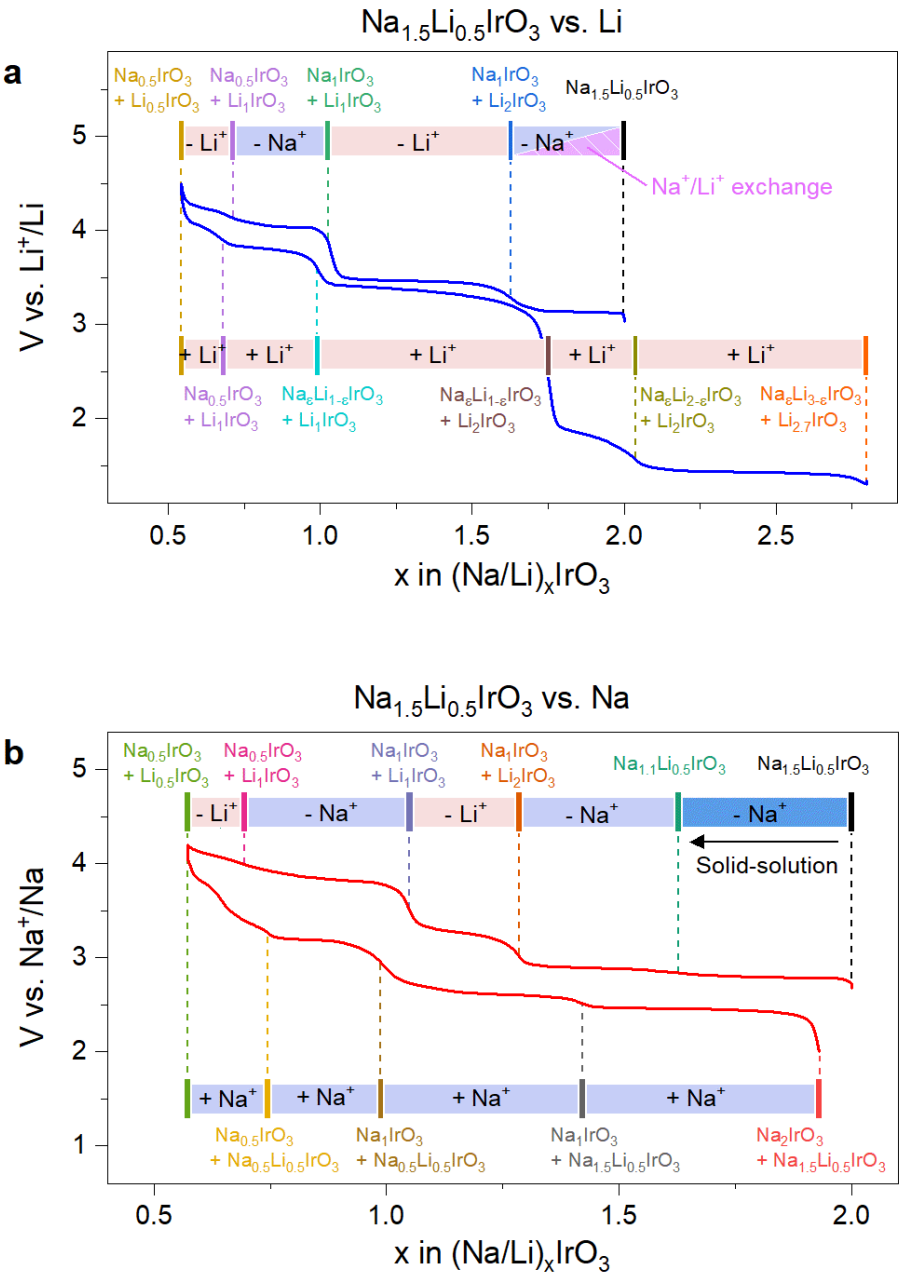

Figure 6 : Overall electrochemical mechanism of $Na_{1.5}Li_{0.5}IrO_3$ in Li and Na batteries. (a) Cycling vs. Li results in ionic exchange between Na in the material and Li from the electrolyte. A small part of the material still contains some sodium after 1 cycle, whereas most of the material turns to Li_2IrO_3, which can insert excess lithium at low voltage. (b) Cycling vs. Na prevents the exchange reaction, revealing a solid-solution mechanism for the deinsertion of the first 0.4 Na^+, but also results in the segregation of Na and Li. After one charge/discharge cycle the material is split between Na_2IrO_3 and a phase close to the pristine $Na_{1.5}Li_{0.5}IrO_3$.

LIST OF TABLES

Table 1. Structural parameters for $Na_{1.5}Li_{0.5}IrO_3$ obtained from Rietveld refinement of synchrotron X-ray and neutron diffraction data.

	$Na_{1.5}Li_{0.5}IrO_3$ - Space group : *C*2/*c*					
	a (Å)	*b* (Å)	*c* (Å)	*β* (°)	χ^2	R_{Bragg}
SXRD	5.33150(5)	9.23324(8)	10.67604(5)	99.5400(8)	17.0	12.8 %
ND	5.3303(5)	9.2257(11)	10.6802(5)	99.664(10)	132	5.81 %
Atom	Wyckoff position	*x/a*	*y/b*	*z/c*	Occupancy	B_{iso} (Å^2)
O1	8*f*	0.594(3)	0.0700(14)	0.1036(11)	1	1.06(5)
O2	8*f*	0.616(3)	0.4237(14)	0.0990(10)	1	1.06(5)
O3	8*f*	0.632(2)	0.753(2)	0.1027(6)	1	1.06(5)
Ir1	8*f*	0.2520(19)	0.0814(5)	0.0045(9)	0.863(4)[a]	1.05(5)
Li1	8*f*	0.2520(19)	0.0814(5)	0.0045(9)	0.137(4) [a]	1.05(5)
Li2	4*d*	0.75	0.25	0	0.725(8) [a]	1.05(5)
Ir2	4*d*	0.75	0.25	0	0.275(8) [a]	1.05(5)
Na3	4*e*	0	0.093(3)	0.25	1	1.87(12)
Na4	4*e*	0	0.430(3)	0.25	1	1.87(12)
Na5	4*e*	0	0.739(4)	0.25	1	1.87(12)

[a] Site mixing between Li and Ir in the 8*f* and 4*d* sites was introduced to artificially reduce the intensity of superstructure peaks.

TOC

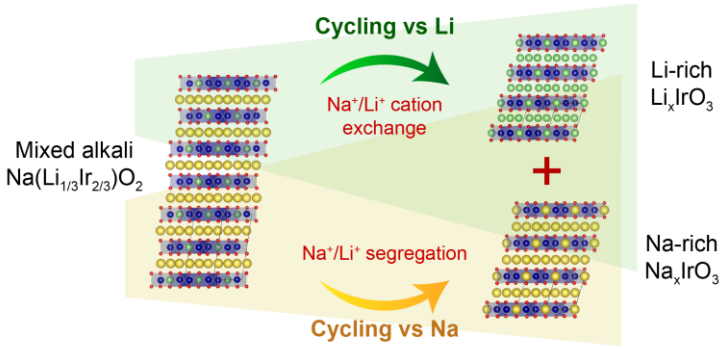

Competition between Na^+/Li^+ deinsertion reactions, cation exchange and segregation leads to the decomposition of the mixed alkali $Na(Li_{1/3}Ir_{2/3})O_2$ into Li-rich Li_xIrO_3 and Na-rich Na_xIrO_3 phases.